Earth Surface Infrared Ultraspectral Emissivity Images Derived from Space-borne Measurements for Environmental Monitoring

Daniel K. Zhou, Allen M. Larar, Xu Liu, and William L. Smith

NASA Langley Research Center, Hampton, VA, USA

Satellite Ultraspectral IR Sounders

Table 1. Characteristics of satellite advanced infrared sounders.

Name	AIRS	IASI	CrIS	IRFS-2	IRS
Orbit	705 km	833 km	824 km	850 km	Geostationary
Instrument type	Grating	FTS	FTS	FTS	FTS
Agency	NASA	EUMETSAT	IPO	RSA	EUMETSAT
Spectral range (cm^{-1})	649–1135 1217–1613 2169–2674	Contiguous 645–2760	650–1095 1210–1750 2155–2550	Contiguous 665–2000	685–1130 1650–2250
Unapodized spectral resolving power ($\nu/\delta\nu$)	1200	2000–4000	1000–1800	2000–4000	2000–4000
Field of view (km)	13	12	14	35	4
Sampling density per 50 km square	9	4	9	1	144
Power (W)	225	200	86	50	300
Mass (kg)	140	230	81	50	200
Platform	Aqua	METOP-1,2,3	NPP NPOESS C1	METEOR	Geostationary
Launch date	2002	2006, 2011, 2017	2011 (NPP) 2013 (C1)	2011	2017

Bill Smith et al. (2009), Technical Note: Evolution, current capabilities, and future advances in satellite ultra-spectral IR sounding, *Atmos. Chem. Phys.*, **9**, 5563–5574

Infrared Atmospheric Sounding Interferometer (IASI) instrument (by CNES/EUMETSAT) on MetOp-A Satellite launched on 19 October 2006

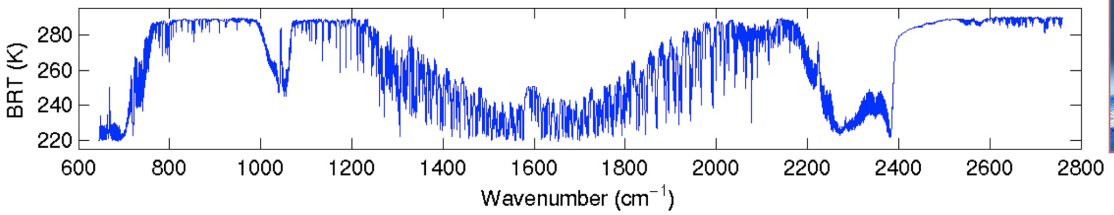

Motivation & Approach

Study Earth from space to improve our scientific understanding of global climate change; derive geophysical parameters of surface and atmosphere from satellite hyperspectral IR measurements.

•Long-term and large-scale observations, needed for global change monitoring and other research, can only be supplied by satellite remote sensing.

•IR hyperspectral radiance measurements are available from current AIRS (since May 2002) and IASI (October 2006), and CrIS will be available from future operational weather satellites.

•Generate an emissivity climatology dataset from satellite data in

1) helping to understand the nature of radiative transfer process for the Earth and atmospheric environment,
2) assisting assimilation of hyperspectral IR radiances in NWP models,
3) improving retrieval accuracy for other thermodynamic parameters (e.g., T_s, T, H_2O, CO, CO_2, O_3 …),
4) helping surface skin temp retrieval from other satellite broad-band measurements (e.g., GOES-R/ABI),
5) improving accuracy of surface radiation budget calculation for climate studies, and
6) long-term monitoring of the global environment and climate change.

Our approach:

•Develop a retrieval algorithm dealing all weather conditions.

•Retrieve surface parameters (e.g., emissivity) and generate the datasets associated with the cloud types.

•We take advantage of the minimal temporary variation of surface emissivity and use the statistical analysis on the emissivity retrieved from clear and cloudy conditions to understand how well infrared sounders observe the atmosphere and surface through clouds.

Hyperspectral Emis. Ret. Algorithms

C. C. Borel (1998): Surface emissivity and temperature retrieval for a hyperspectral sensor, *Geoscience and Remote Sensing Symposium Proceedings*, 1, 546-549.

D. K. Zhou et al. (2002): Thermodynamic product retrieval methodology for NAST-I and validation, *Appl. Opt.*, 41, 6957–6967.

R. O. Knuteson et al. (2004): Infrared land surface remote sensing using high spectral resolution aircraft observations, *Advances In Space Research*, 33 1114–1119.

J. Li et al. (2007): Physical retrieval of surface emissivity spectrum from hyperspectral infrared radiances, *Geophys. Res. Lett.*, 34, L16812.

L. Zhou et al. (2008): Regression of surface spectral emissivity from hyperspectral instruments, *IEEE Trans. Geosci. Remote Sensing*, 46, 328–333.

J. Susskind et al. (2008): Improved surface parameter retrievals using AIRS/AMSU data, *Proc. SPIE*, 6966, 10–12.

E. Péquignot et al. (2008): Infrared Continental Surface Emissivity Spectra Retrieved from AIRS Hyperspectral Sensor, *J. Appl. Meteorol. Climatol.*, 47, 1619–1633.

X. Liu et al. (2009): Retrieval of atmospheric profiles and cloud properties from IASI spectra using super-channels, *Atmos. Chem. Phys.*, 9, 9121–9142.

D. K. Zhou at al. (2011): Global land surface emissivity retrieved from satellite ultraspectral IR measurements, submitted to *IEEE Trans. Geosci. Remote Sensing,* **49**, 1277–1290.

IR-only Retrieval Algorithm

Part A: Regression Retrieval (*Zhou et al.*, GRL 2005)

Using an all-seasonal-globally representative training database to diagnose 0-2 cloud layers from training relative humidity profile:

A single cloud layer is inserted into the input training profile. Approximate lower level cloud using opaque cloud representation.

Use parameterization of balloon and aircraft cloud microphysical data base to specify cloud effective particle diameter and cloud optical depth:

Different cloud microphysical properties are simulated for same training profile using random number generator to specify visible cloud optical depth within a reasonable range. Different habitats can be specified (Hexagonal columns assumed here).

Use LBLRTM/DISORT "lookup table" to specify cloud radiative properties:

Spectral transmittance and reflectance for ice and liquid clouds interpolated from multi-dimensional look-up table based on DISORT multiple scattering calculations.

Compute EOFs and Regressions from clear, cloudy, and mixed radiance data base:

Regress cloud, surface properties & atmospheric profile parameters against radiance EOFs amplitudes.

Part B: 1-D Var. Physical Retrieval (*Zhou et al.*, JAS 2007)

A one-dimensional (1-d) variational solution with the regularization algorithm is used for physical retrieval methodology which uses the regression solution as the initial guess.

Cloud optical and microphysical parameters, namely effective particle diameter and visible optical thickness are further refined with the radiances observed within the 10.4 to 12.5 μm window.

Emissivity (ε_ν) is linear to Radiance (R_ν)

$$R_\nu = \varepsilon_\nu B_\nu(T_s)\tau_\nu(p_s \to 0, \theta_{sat}) + \int_{p_s}^{0} B_\nu[T(p)] \frac{d\tau_\nu(p \to 0, \theta_{sat})}{dp} dp$$

$$+ F_\nu^d \rho_\nu^t \tau_\nu(p_s \to 0, \theta_{sat}) + \frac{H_\nu}{\sec(\theta_{sun})} \tau_\nu(0 \to p_s, \theta_{sun}) \rho_\nu^s \tau_\nu(p_s \to 0, \theta_{sat})$$

$$= [\int_{p_s}^{0} B_\nu[T(p)] \frac{d\tau_\nu(p \to 0, \theta_{sat})}{dp} dp + F_\nu^d \tau_\nu(p_s \to 0, \theta_{sat}) + \frac{H_\nu}{\sec(\theta_{sun})\pi} \tau_\nu(0 \to p_s, \theta_{sun}) \tau_\nu(p_s \to 0, \theta_{sat})]$$

$$+ [B_\nu(T_s)\tau_\nu(p_s \to 0, \theta_{sat}) - F_\nu^d \tau_\nu(p_s \to 0, \theta_{sat}) - \frac{H_\nu}{\sec(\theta_{sun})\pi} \tau_\nu(0 \to p_s, \theta_{sun}) \tau_\nu(p_s \to 0, \theta_{sat})] \varepsilon_\nu$$

$$= k_1 + k_2 \varepsilon_\nu$$

The surface is assumed to be Lambertian (or diffuse reflection

$\rho_\nu^t =$ spectral surface reflectivity, $(1 - \varepsilon_\nu)$

$\rho_\nu^s =$ spectral solar reflectivity, $(1 - \varepsilon_\nu)/\pi$

$R_\nu =$ observed spectral radiance

$\varepsilon_\nu =$ spectral emissivity

$B_\nu =$ spectral Planck function

$T_s =$ surface skin temperature

$\tau_\nu(p_1 \to p_2) =$ spectral transmittance from pres p_1 to p_2

$T(p) =$ temperature at pressure p

$H =$ solar irradiance

$\theta_{sun} =$ solar zenith angle

$\theta_{sat} =$ sattlite zenith angle

$F_\nu^d =$ down welling thermal flux

Training Dataset & Emissivity Regression

Atmospheric : An all-seasonal-globally representative training database (UW SeeBor Database).

Surface : $T_s=T_a+T_\delta$, where T_δ is a random number generated value with a mean of 0 K and a STD of 3 K over water and 10 K over land. ε is randomly assigned to profile from ε database.

Cloud : Use parameterization of balloon and aircraft cloud microphysical data base to specify cloud effective particle size and cloud optical depth using random number generator to specify visible cloud optical depth within a reasonable range.

$$F(\varepsilon_\nu)=\log[\log(\varepsilon^{HB}-\varepsilon^{LB}+\delta)-\log(\varepsilon^{HB}-\varepsilon_\nu)]$$

- Lab. measured emis. converted to emis. logarithm function $F(\varepsilon)$ to constrain emis. retrieval.

$$A_i^F=\sum_{j=1}^{nch}F_j(\varepsilon)\varphi_{ji}^F$$

- A set of emis. logarithm functions are used to calculate its Eigenvectors and their amplitudes. Emis. amplitudes are used with other other parameters as a state vector to calculate radiance.

$$A_i=\sum_{j=1}^{nc}R_j\varphi_{ji}$$

- A set of radiances are used to calculate its Eigenvectors and their amplitudes.

$$S_j=\sum_{i=1}^{n-1}K_{ji}A_i+K_{jn}P_s=\sum_{i=1}^{n-1}K_{ji}(\sum_{l=1}^{nc}R_l\varphi_{li})+K_{jn}P_s$$

- Regression coefficients are generated using a training database (state vector) and their associated radiances. State vector is retrieved with measured radiance. Emis. EOF amplitudes are part of the state vector.

$$\varepsilon_j=\varepsilon^{HB}-\exp[\log(\varepsilon^{HB}-\varepsilon^{LB}+\delta)-\exp(F_j)]$$

$$=\varepsilon^{HB}-\exp[\log(\varepsilon^{HB}-\varepsilon^{LB}+\delta)-\exp(\sum_{i=1}^{9}\varphi_{ji}^F A_i^F)]$$

- Emissivity spectrum is calculated with retrieved emis. EOF amplitudes.

Cloud Detection within Retrieval

Multi-stage regression retrievals are performed. The first-stage involves mixed (i.e., clear and cloudy) regression. The second-stage (e.g., either clear or cloudy) depends on the cloud detection criteria that are based on first-stage retrieved cloud parameters.

Note: ϕ = 0, 1, and 2 are for clear sky, ice cloud, and water clouds, respectively; and H_c is cloud top height relative to surface, ϕ is cloud phase, and τ_{cld} is cloud visible optical depth.

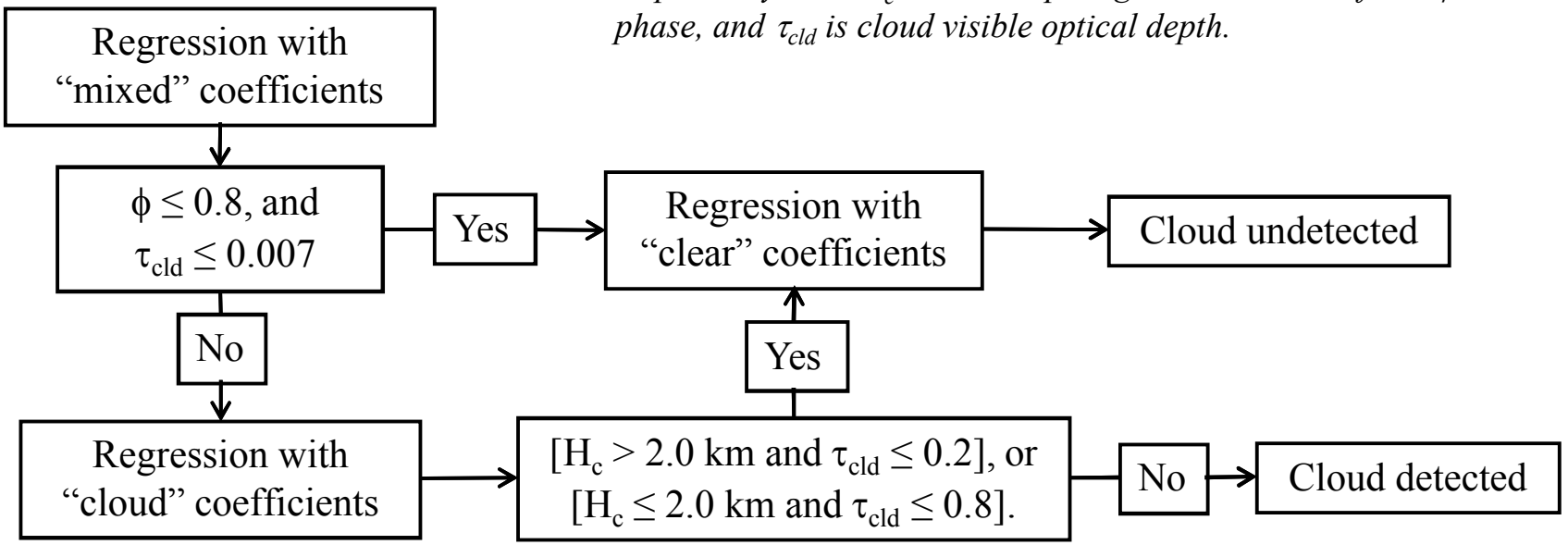

IASI Derived LST (Temporal)

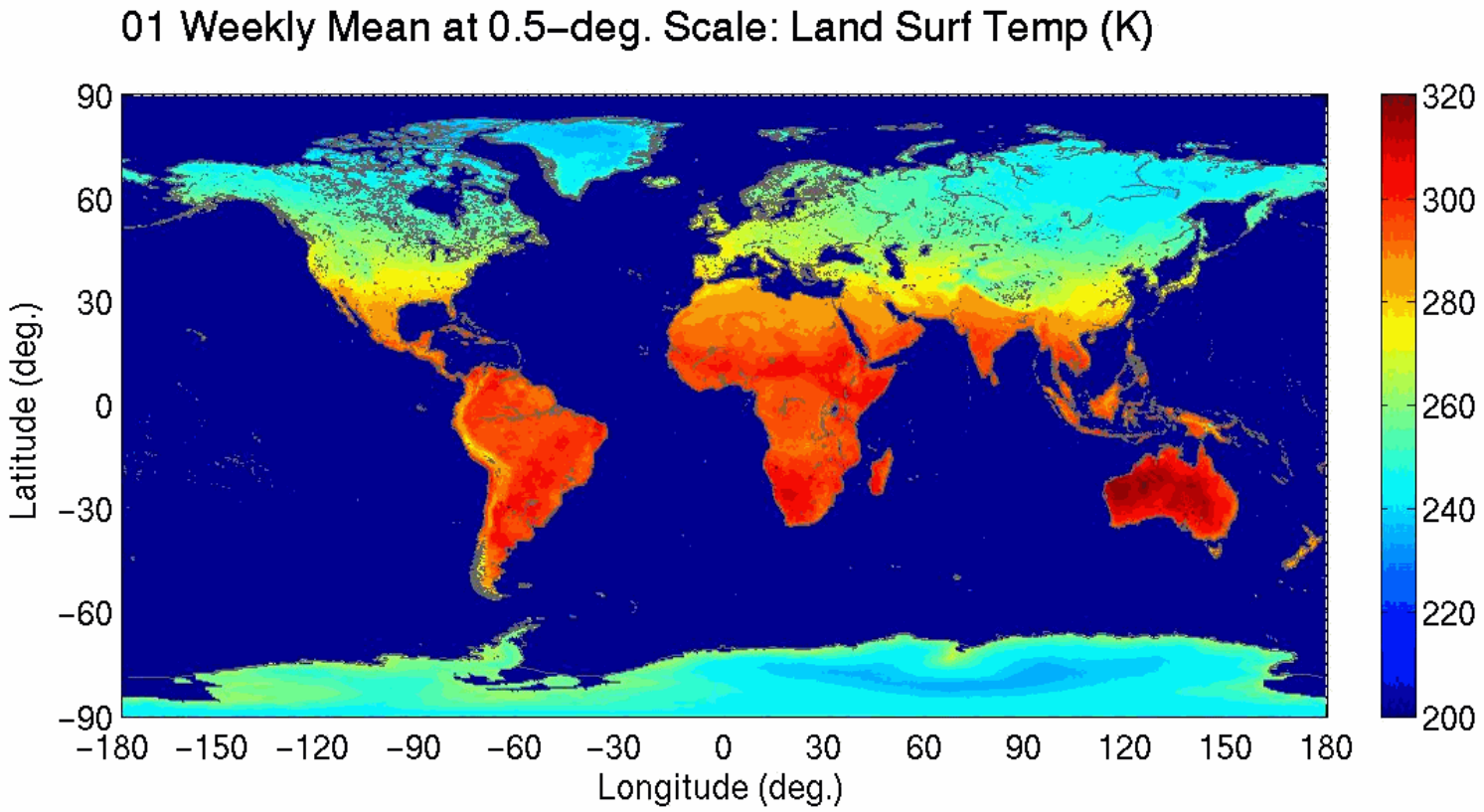

IASI Derived 4-D LSE (temporal)

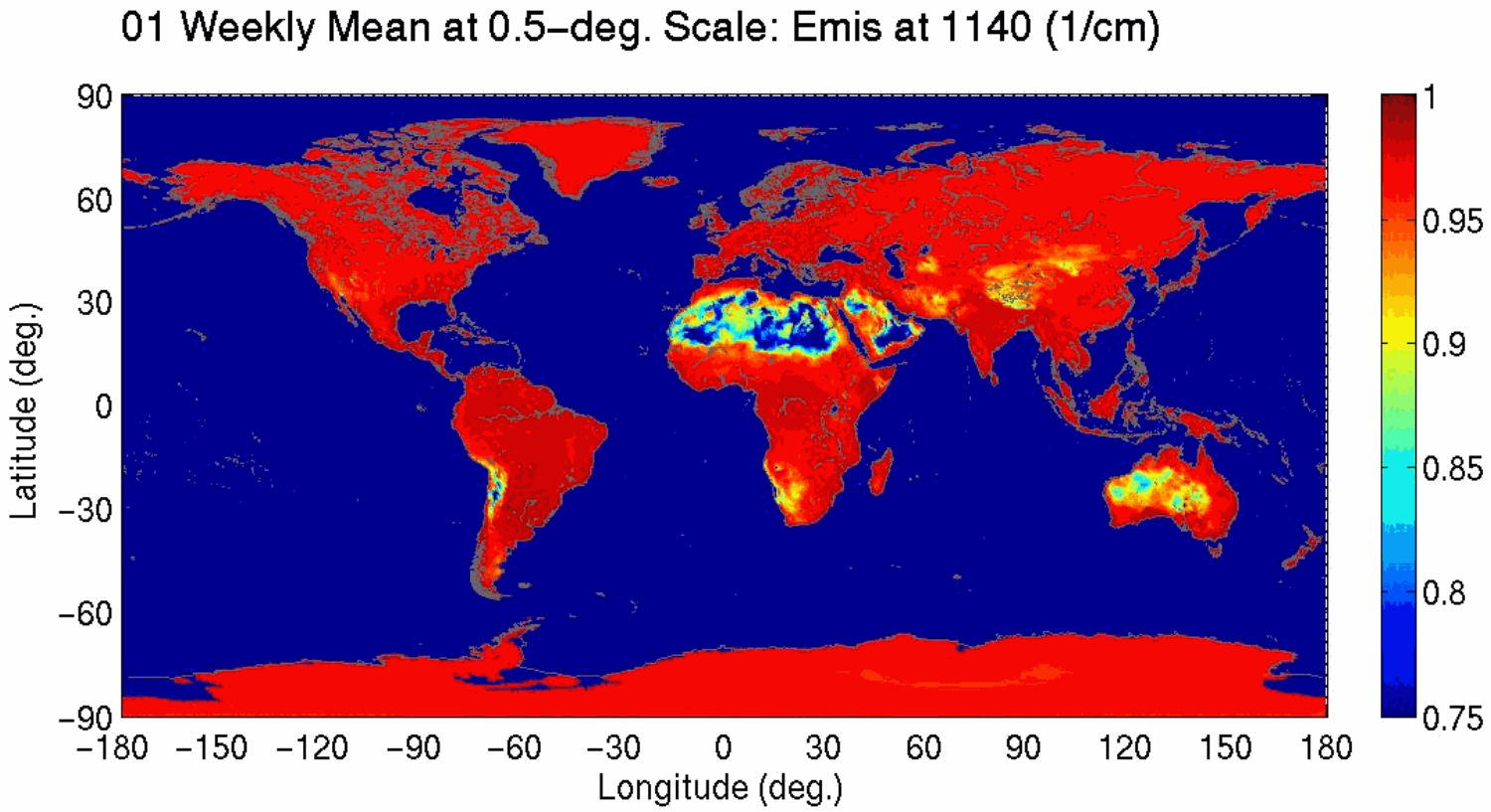

LSE Seasonal Variation (950 cm^{-1})

Each spring after a cold, sunny, windy, and dry winter, sandstorms strike Northern China and the yellow dust migrates from China's interior (the Gobi and Ordos deserts) to its capital, Beijing, and eastern seaboard, thus decreasing the emissivity over wide regions while the ground is still very dry with minimum rainfall in the winter and early spring seasons.

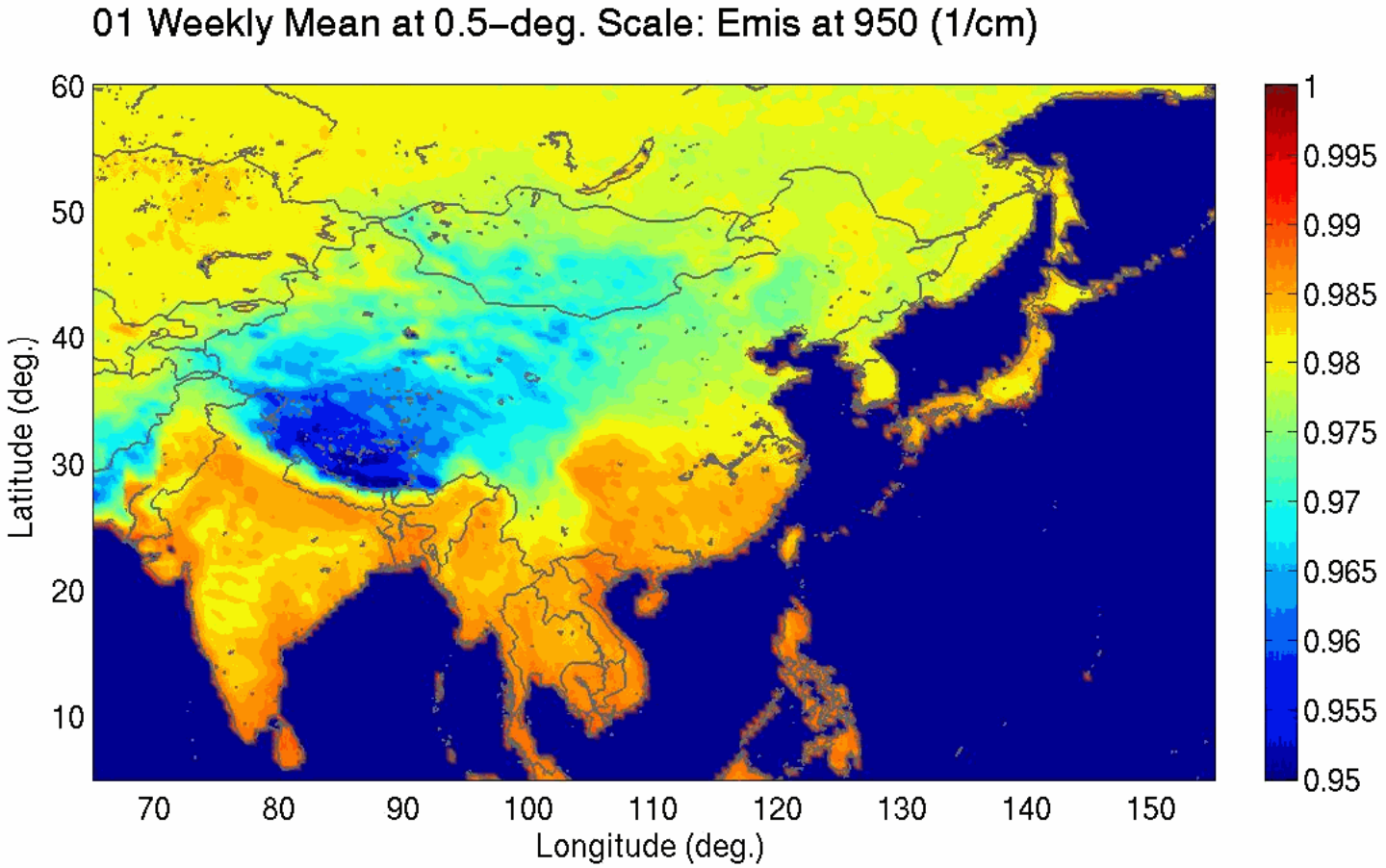

LSE Seasonal Variation (950 cm^{-1})

The emissivity variation is coherent, which indicates that the emissivity variation is associated with seasonal changes of the weather or surface weather (i.e., rainfall modifying soil moisture or snowfall accumulating on the surface) and the varying ground cover with a different vegetation coverage.

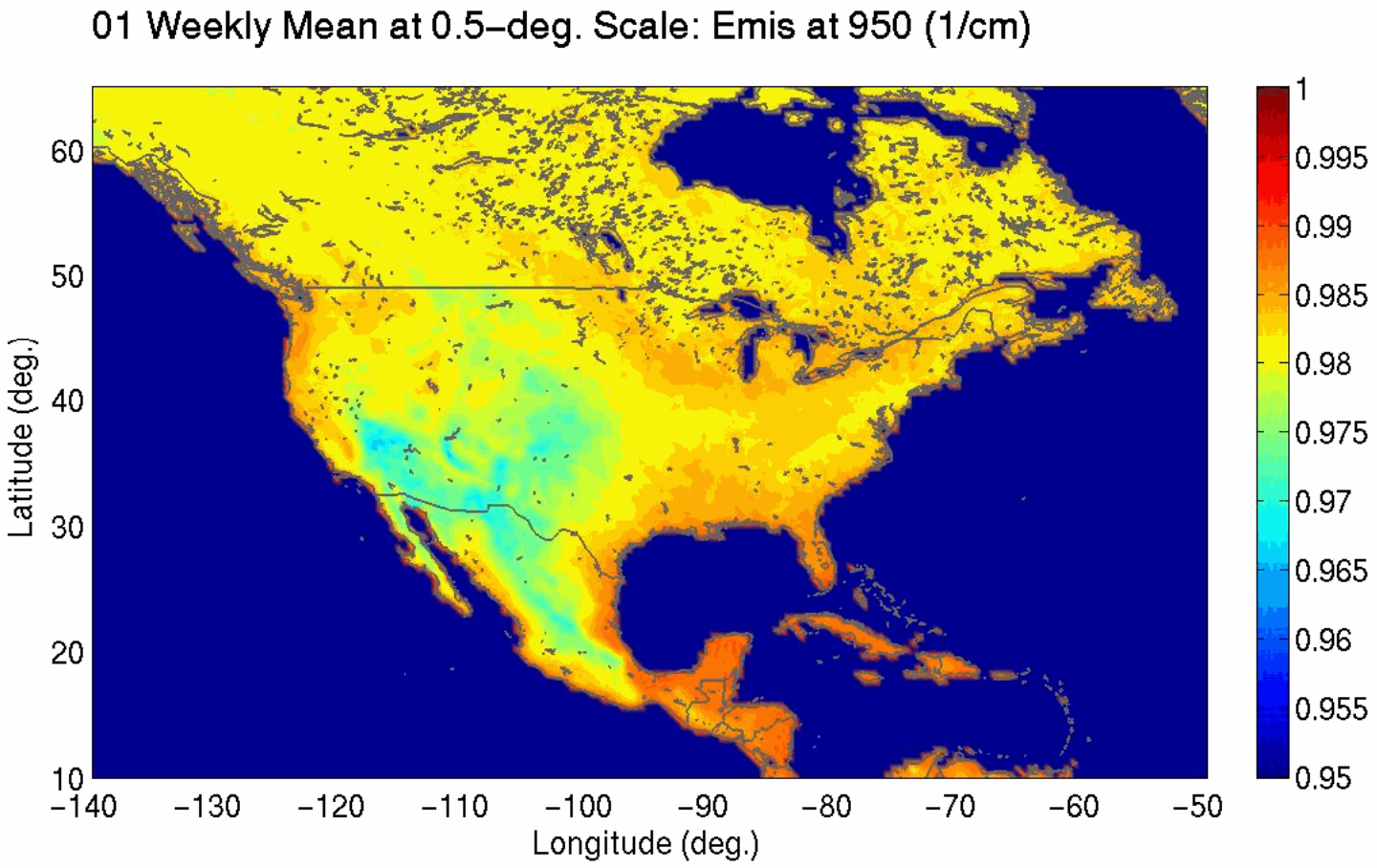

IASI Derived 4-D LSE (Spectral)

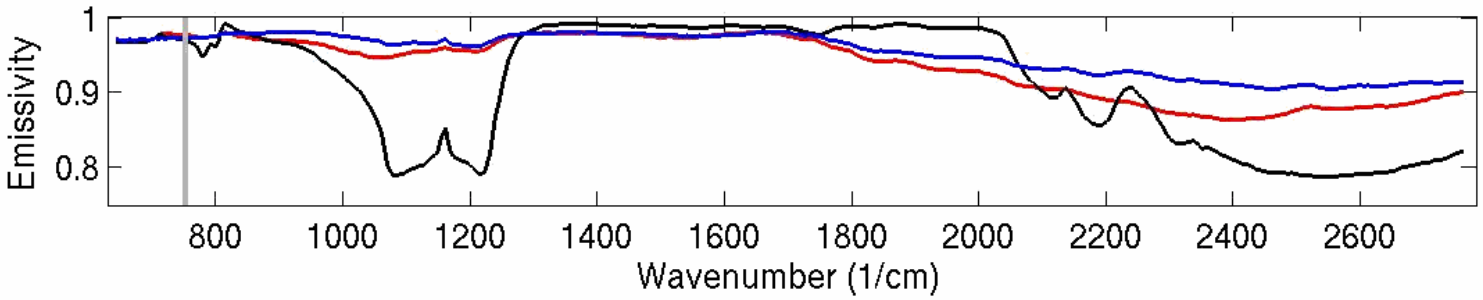

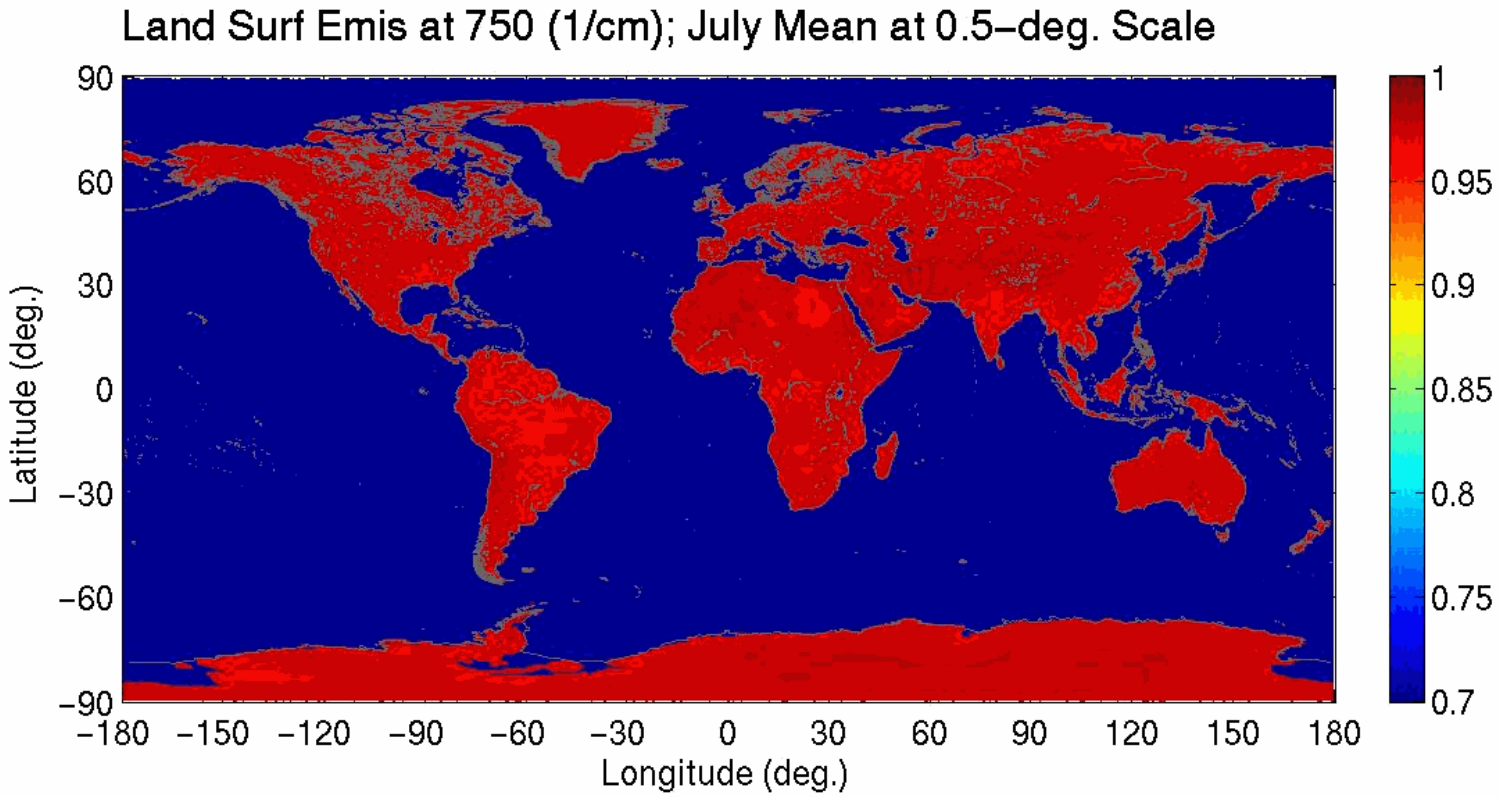

Emis. Accuracy Estimation Under Clear-sky

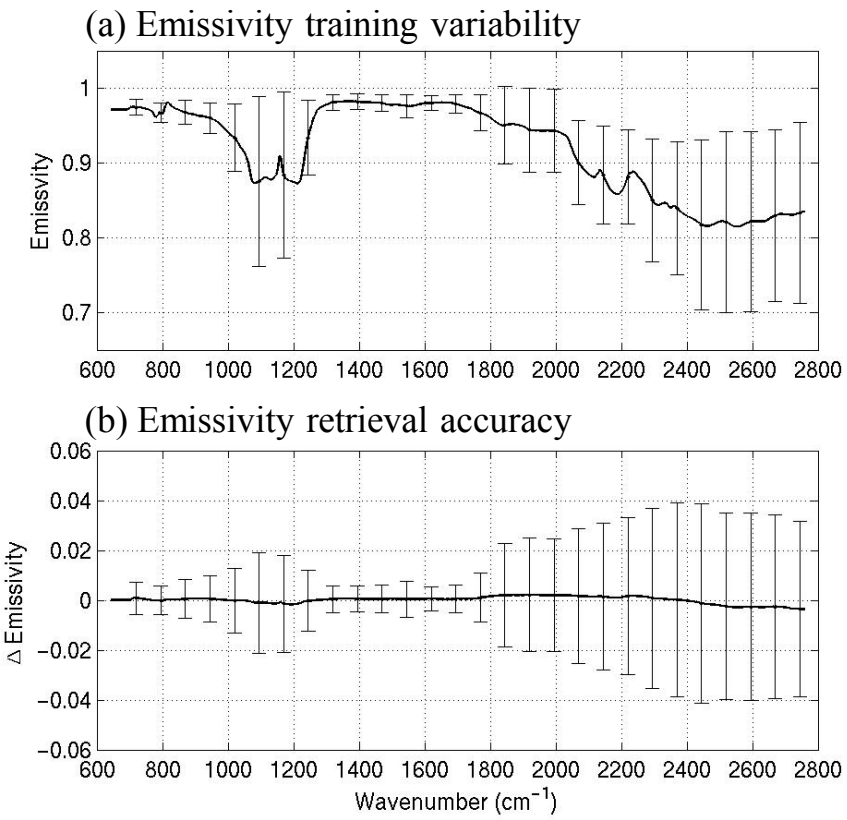

- The emissivity assigned to each training profile is randomly selected from a laboratory measured emissivity database, indicated in panel **a**, and has a wide variety of surface types suitable for different geographical locations. The vertical bars show the emissivity STD for this dataset.
- Estimated surface emissivity retrieval accuracy, the mean difference (or bias) in curve and the STDE in vertical bars shown in panel **b**, is training data dependent.
- Surface skin temperature is one of the most "coupled" parameters with emissivity, it is necessary to mention that skin temperature retrieval accuracy has a -0.035 K bias with a 1.11 K STDE from the same analysis

Note: since the emissivity is linear to channel radiances, we chose to use retrieved emissivity from linear EOF regression, not further retrieved in physical iteration. However, if the physical retrieval is performed for other parameters, emissivity will be further refined through physical iteration.

Emis. Ret. and Rad. Fitting Samples

Over Sahara (Lat.=23.38° N; Lon.=24.41° E);
Daytime (SZA=30.5°), 2007.08.01

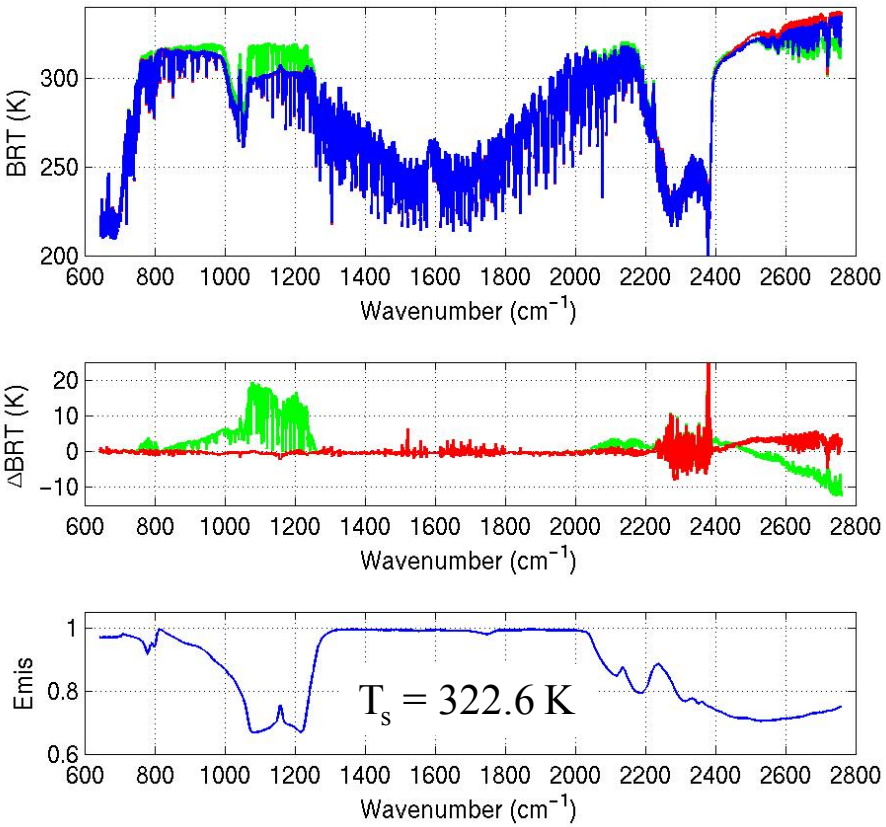

Over Sahara (Lat.=23.41° N; Lon.=24.83° E);
Nighttime (SZA=120.6°), 2007.08.01

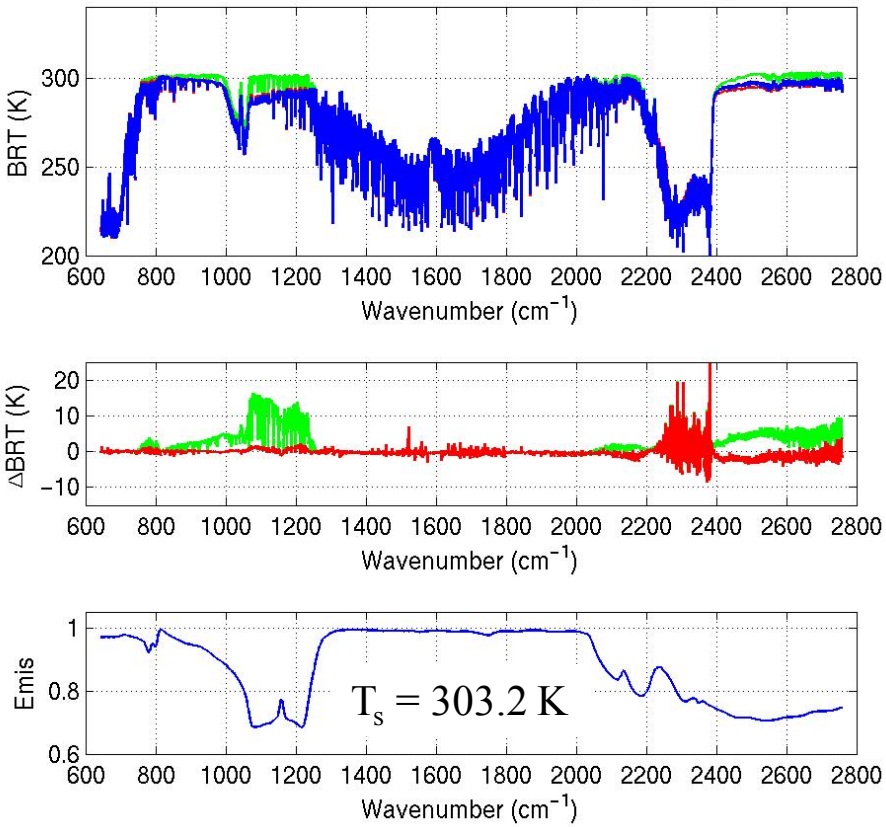

It demonstrates that the technique separates surface emissivity from skin temperature:
Samples shown are for both day and night observations over the Sahara Desert. Simulated spectral radiances (with rtv emis in red curves; emis of 1 in green curves) are plotted in comparison with the measurements (blue curves). Retrieved surface emissivity spectra are plotted in the bottom panels with IASI day and night observations, respectively.

Namib and Kalahari Deserts for Validation

Namib: Lat.= 26.35 S, Lon.=20.7 E

Kalahari: Lat.= 24.75 S, Lon.=15.3 E

Namib and Kalahari Deserts for ε Validation

G. C. Hulley, S. J. Hook, E. Manning, S.-Y. Lee, and E. Fetzer, "Validation of the Atmospheric Infrared Sounder (AIRS) version 5 land surface emissivity product over Namib and Kalahari deserts," *J. Geophys. Res.*, vol. 114, no. D1, pp. 9104.1–9104.11, Oct. 2009.

- **Kalahari:** The majority of the sand lies on the level plains of the Kalahari Basin, sand dunes mixed with grassy scrublands and sparse trees.

- **Namib:** The vast expanse of shifting dunes is almost completely devoid of vegetation except for sparse perennial grasses.

- Different sand mineralogy from Namib to Kalahari sites.

Table 1. Summary of the Major Characteristics of the Kalahari and Namib Validation Sites Including Locality, Elevation, Surface Area, Dune Height, Grain Size, Sand Source and Bulk Mineralogy

	Kalahari	Namib
Locality	covers most of Botswana, including northwestern South Africa and southeastern Namibia	western coast of Namibia
Approximate surface area (km^2)	100,000	34,000
Elevation (m)	1,000	0–500
Maximum dune height (m)	30	300
Percent of grain size of sand		
>500 μm	0%	1%
250–500 μm	30%	53%
125–250 μm	68%	40%
<125 μm	2%	6%
Sand source	aeolian deposited, fluvial	littoral, fluvial, weathered tsondab sandstone
Mineralogy		
Major	Quartz	quartz
Minor		feldspar, magnetite

Emissivity Validation / Evaluation

- We will use the Namib site for absolute validation and the Kalahari site for relative spectral-shape validation.

- The quartz-doublet region from the Namib to the Kalahari site, is well captured by retrievals, due to the different sand mineralogy at these 2 sites.

Kalahari Site

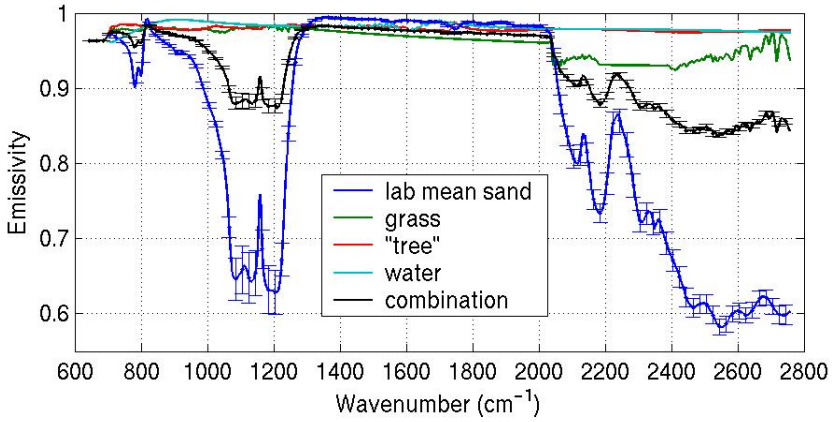

Namib Site

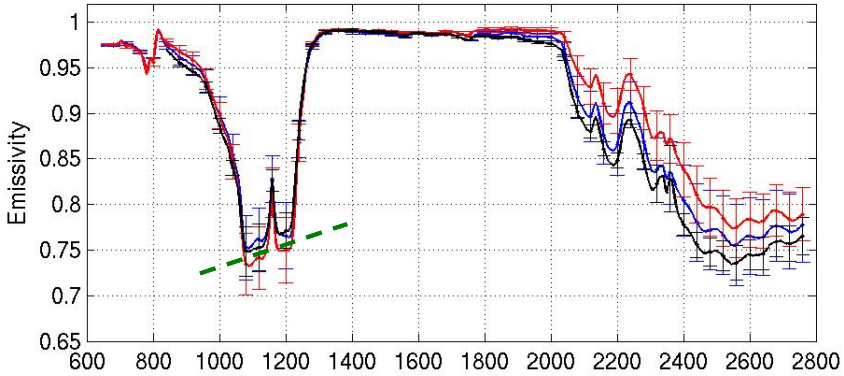

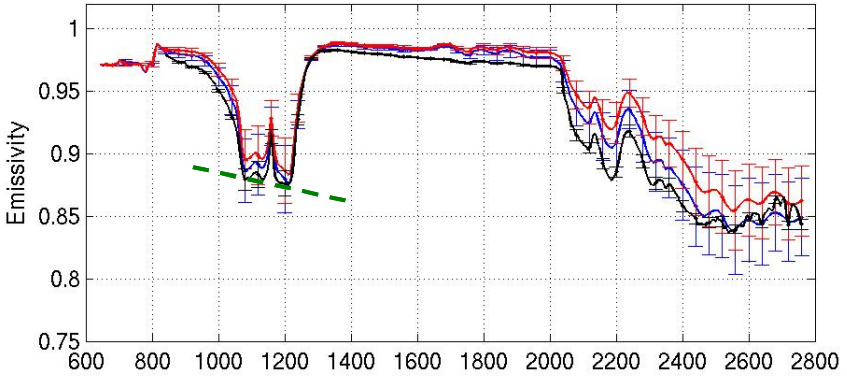

Land Surface Skin Temp. Monitoring

Samples from the Arctic:
Lat. = 77.9±1.0 N
Lon. = 43.6±1.0 W
Alt. ≈ 2.56 km.

Samples from the Safari:
Lat. = 24.5±0.2 N
Lon. = 13.0±0.2 E
Alt. ≈ 0.68 km.

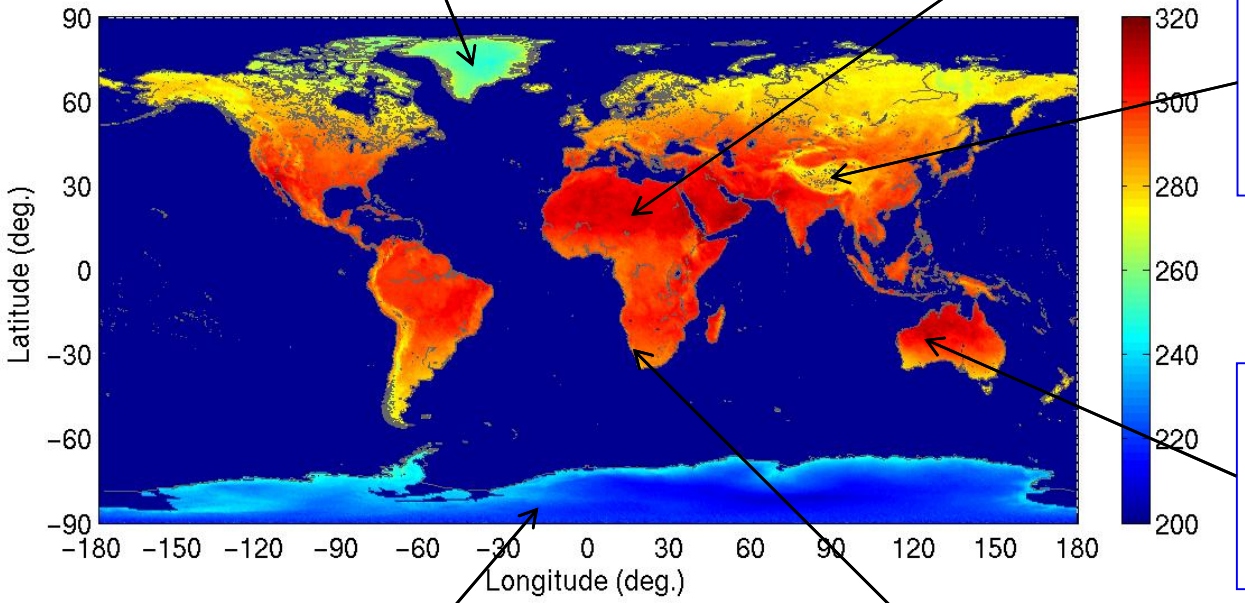

Samples from the Tibetan Plateau:
Lat. = 32.4±0.5 N,
Lon. = 85.1±0.5 E,
Alt. ≈ 5.26 km.

Samples from the Gibson Desert:
Lat. = 22.5±0.5 S
Lon. = 123.0±0.5 E
Alt. ≈ 0.27 km.

Samples from the Antarctic:
Lat. = 80.0±1.0 S
Lon. = 110.0±1.0 W
Alt. ≈ 1.45 km.

Samples from the Nambi:
Lat. = 24.75±0.2 S
Lon. = 15.3±0.2 E
Alt. ≈ 0.56 km.

Langley Research Center

Land Surface Skin Temp. Monitoring

Samples from the Arctic:
Lat. = 77.9±1.0 N
Lon. = 43.6±1.0 W
Alt. ≈ 2.56 km.

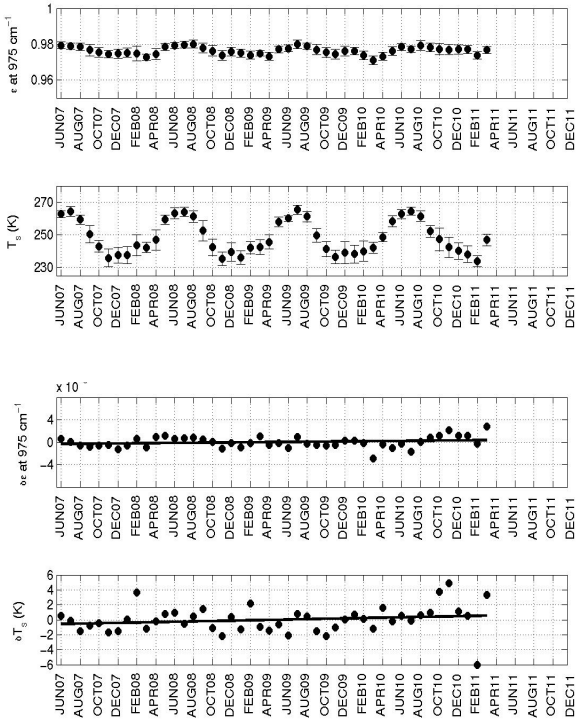

T_s trend linear fitting:

$T_s = 0.025m - 0.60$,

T_s increase 0.025 K/mon.
(or 0.30 K/year).

Samples from the Tibetan Plateau:
Lat. = 32.4±0.5 N,
Lon. = 85.1±0.5 E,
Alt. ≈ 5.26 km.

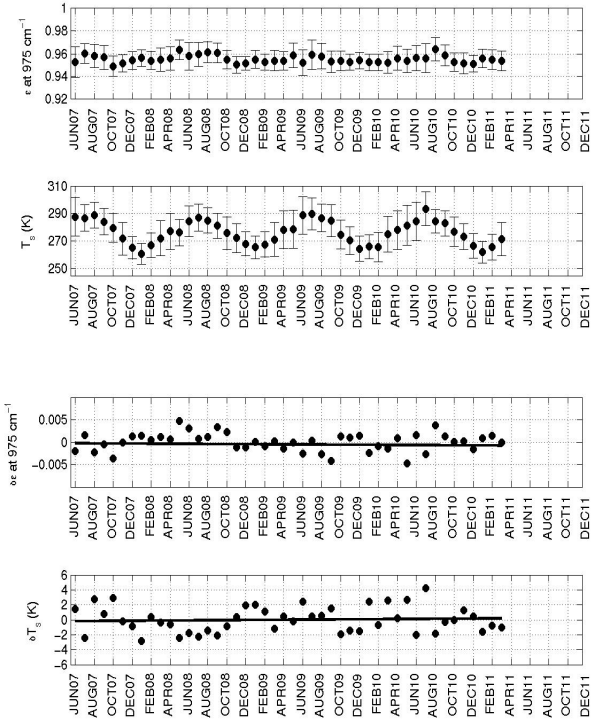

T_s trend linear fitting:

$T_s = 0.0081m - 0.19$,

T_s increase 0.0081 K/mon.
(or 0.10 K/year).

Samples from the Antarctic:
Lat. = 80.0±1.0 S
Lon. = 110.0±1.0 W
Alt. ≈ 1.45 km.

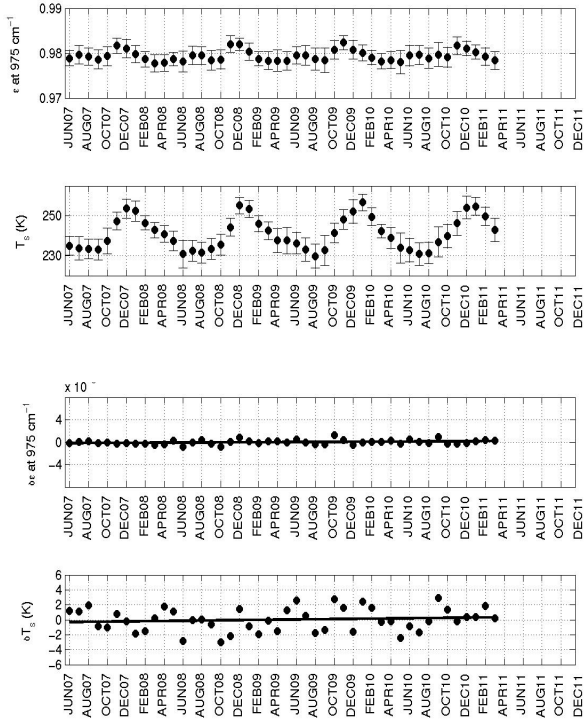

T_s trend linear fitting:

$T_s = 0.014m - 0.32$,

T_s increase 0.014 K/mon.
(or 0.17 K/year).

Langley Research Center

Land Surface Skin Temp. Monitoring

Samples from the Gibson Desert:
Lat. = 22.5±0.5 S
Lon. = 123.0±0.5 E
Alt. ≈ 0.27 km.

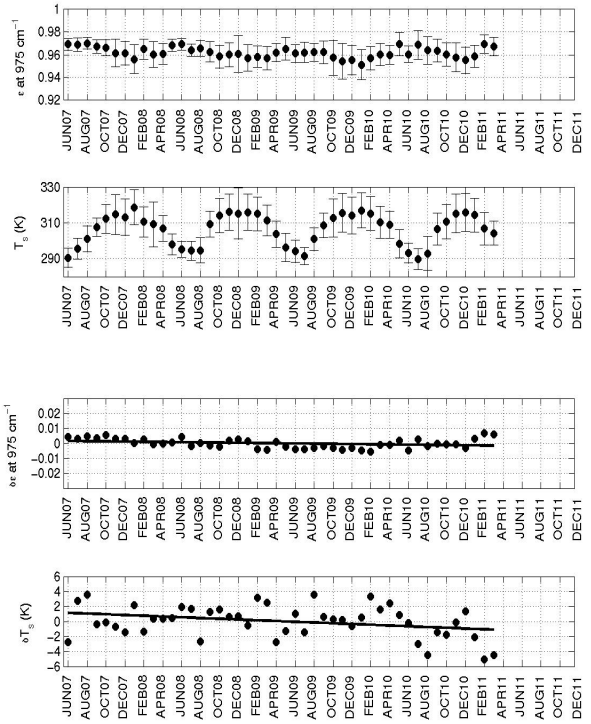

T_s trend linear fitting:

T_s = -0.025m + 0.12 ,

T_s decrease 0.025 K/mon.
(or -0.3 K/year).

Samples from the Safari:
Lat. = 24.5±0.2 N
Lon. = 13.0±0.2 E
Alt. ≈ 0.68 km.

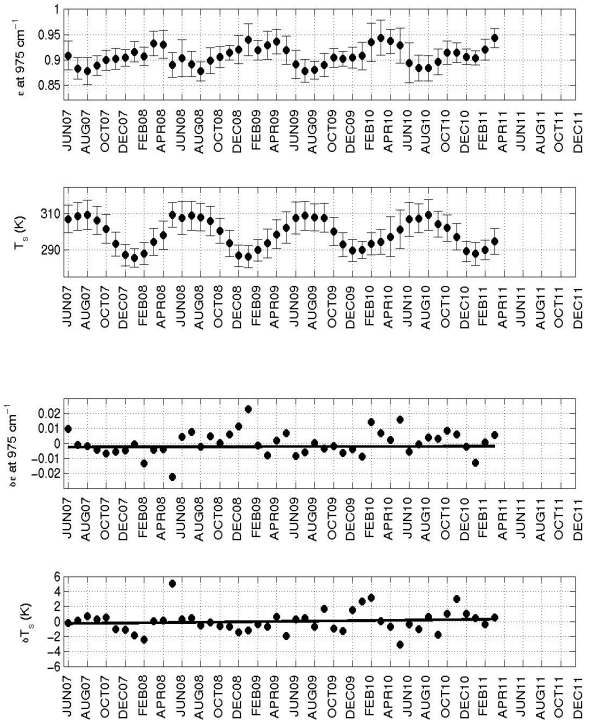

T_s trend linear fitting:

T_s = 0.013m – 0.31 ,

T_s increase 0.013 K/mon.
(or 0.16 K/year).

Samples from the Nambi:
Lat. = 24.75±0.2 N
Lon. = 15.3±0.2 E
Alt. ≈ 0.56 km.

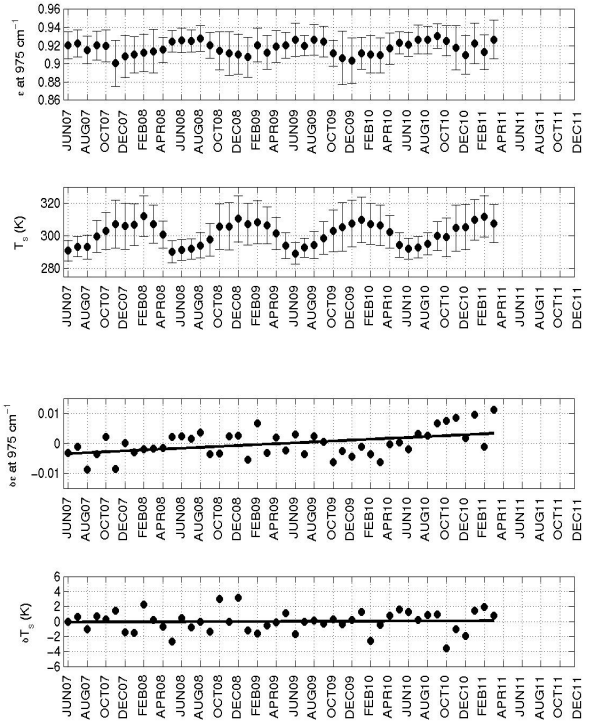

T_s trend linear fitting:

T_s = 0.0039m – 0.092 ,

T_s increase 0.0039 K/mon.
(or 0.05 K/year).

Global Surface Monitoring

Skin temperate trend (K/year):
global mean = -0.0154 (K/year)

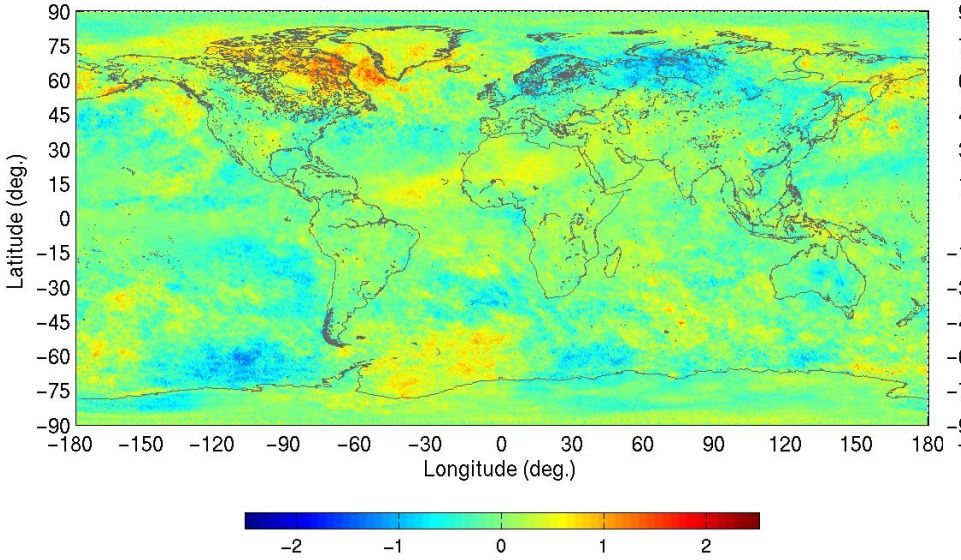

Emissivity trend at 975 cm^{-1} (10^{-3}/year)
global mean = 4.794×10^{-5} (1/year)

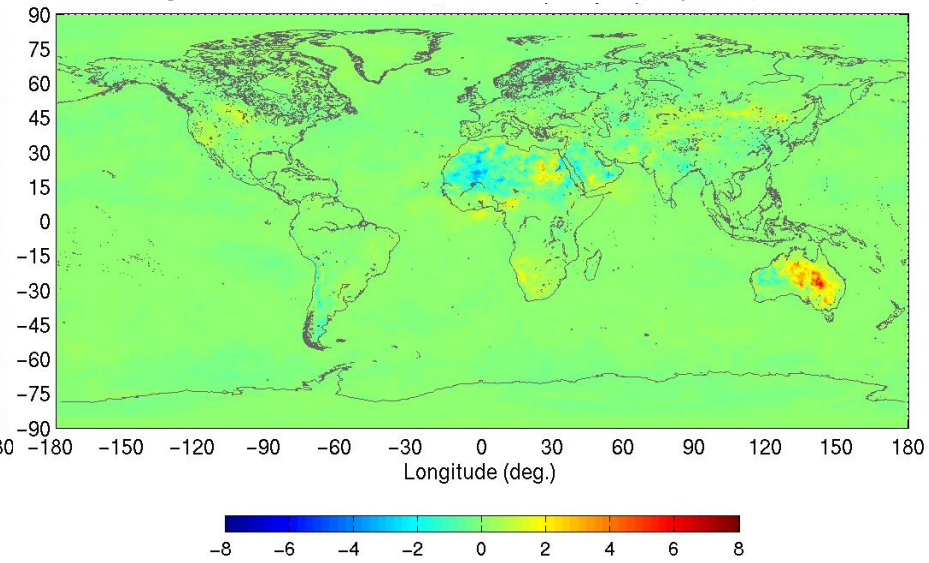

Note:

1. IASI nighttime data are from **June 2007 to April 2011** processed in the 0.5 × 0.5 deg. lat.-long. grid with monthly mean.
2. We take the advantage of the global processing is to view global distribution image of surface skin temperature warming and/or cooling.

Global Land / Water Surface Monitoring

Skin temperate trend (K/year):
global land mean = 0.0047 (K/year)

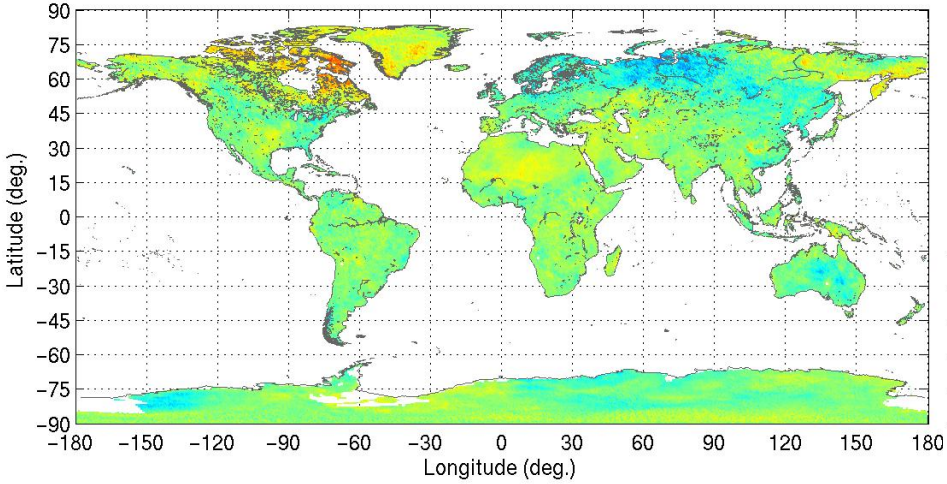

Emissivity trend at 975 cm^{-1} (10^{-3}/year)
global land mean = 5.484×10^{-5} (1/year)

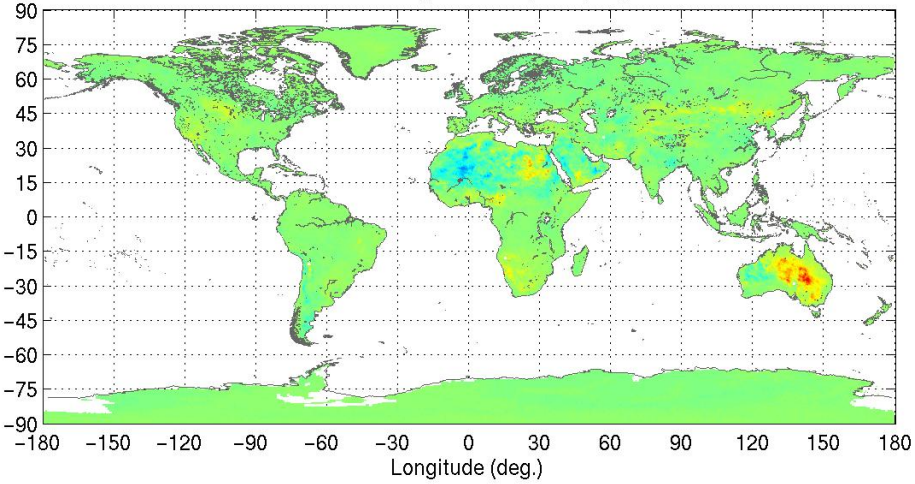

Skin temperate trend (K/year):
global water mean = -0.0290 (K/year)

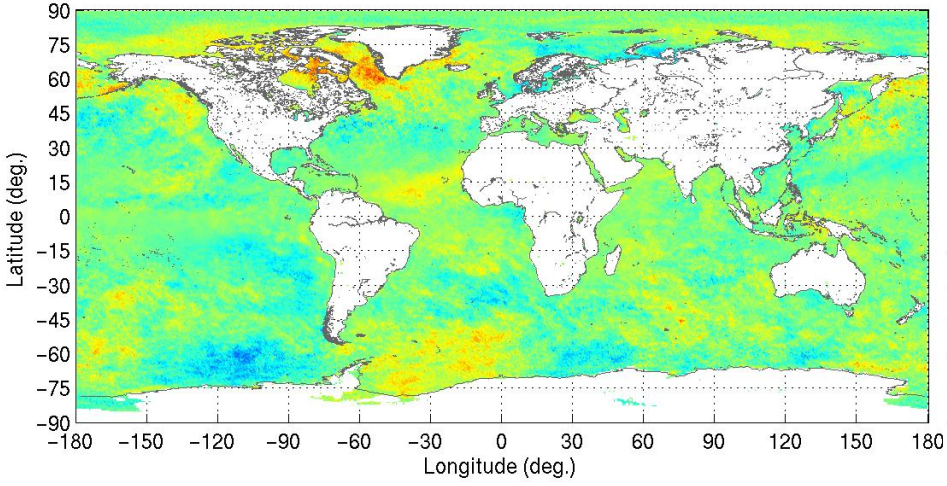

Emissivity trend at 975 cm^{-1} (10^{-3}/year)
global water mean = 4.704×10^{-5} (1/year)

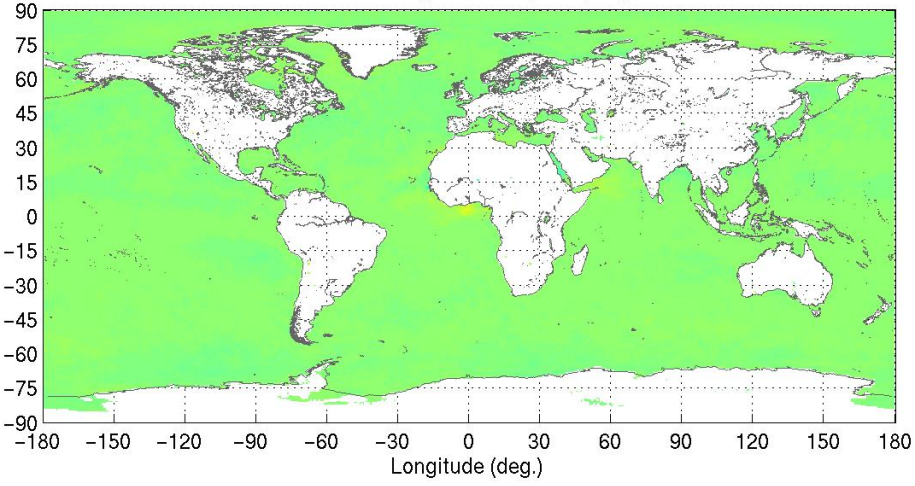

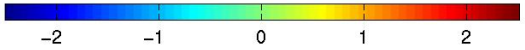

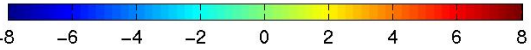

Summary

- A state-of-the-art retrieval algorithm, dealing with all-weather conditions, has been developed and applied to IASI radiance measurements. Surface emissivity is retrieved using multi-stage linear EOF physical-regressions.
- Initial emissivity validation over the Namib and Kalahari deserts is performed. IASI Emissivity retrieval accuracy under clear-sky conditions is estimated that a STDE is about 0.02 and 0.04 for longwave and shortwave window regions, respectively.
- Results from IASI retrievals indicate that surface emissivity retrieved with satellite IR ultraspectral data can capture different land surface type properties. The seasonal and diurnal variation of global land surface emissivity derived from satellite IR ultraspectral data is evident.
- Preliminary global distributions of surface skin temperature and emissivity trends are produced and will be extended for further global monitoring and investigation.